Supporting Information

SP1. Korean geoinformation and land cover type

South Korea (33°–39°N, 124°–130°E) is a mountainous country, with high mountains, hills and valleys. Extended plains surround main river branches on the western side of the Korean Peninsula. Land-use type in 2011 was generally categorized into agriculture (i.e., upland crop, paddy rice, orchard, and other plantation), residential, forestry and grassland areas (Figure S1), which are found in both low and high elevation areas. Coverages of forest, paddy rice fields, dry crop fields, and other land-cover classes are 64.2%, 10.0%, 8.3%, and 17.5%, respectively. The country tends to have a humid continental climate, and is affected by the East Asian monsoon prevailing from June to September, during which > 50% of annual precipitation falls. Annual average temperature varies between 10 and 16ºC, and annual precipitation between 1000 and 1800 mm. The Charyeong rice plain (99.5 km L×58.5 km W, the region encompassed by a white line in Figure S1) is the largest rice-cropping area that supplies more than a half of the rice production in South Korea.

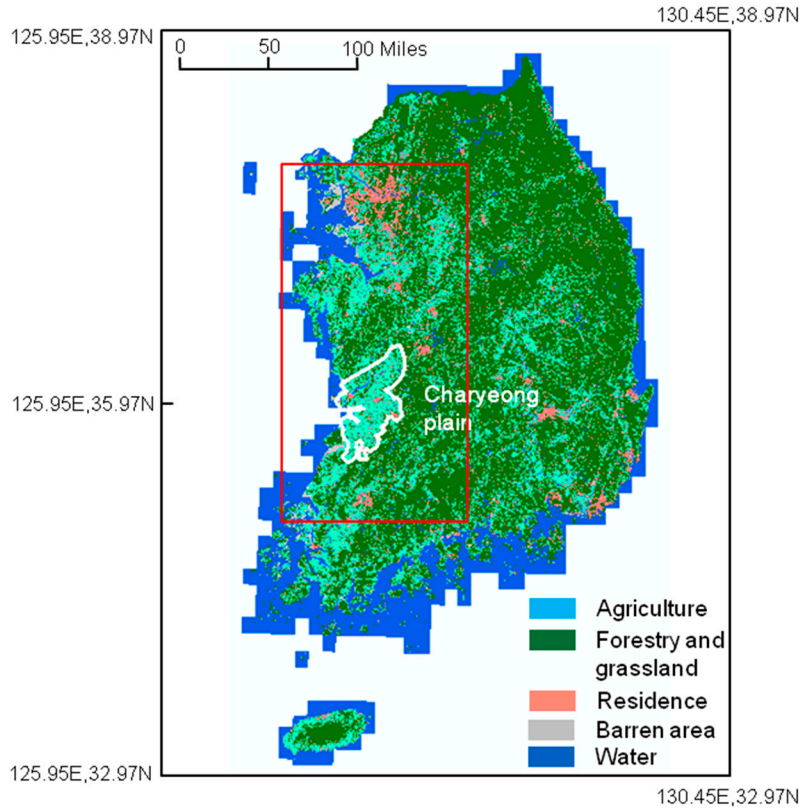

Figure S1. 5-m resolution raster image of main land-cover types in 2011, South Korea (revised from Jeong et al., 2012). Land area enclosed by thick white line is Charyeong rice plain, the largest rice cropping area. Land area enclosed by red square is area of interest for land surface air temperature comparison between paddy fields and the temperate forest.

Rice land use from 1995 to 2017 in main great plain of Western Korea showed a general tendency of decrease, in line with statistical analysis of paddy rice land use of the entire country (Figure S2). Paddy rice land use in 2011 similar to that of 2012 implies that the land-use and classification map of Korea at 5-m

resolution (cf. Figure S1) constructed in 2011 is a valuable reference for analyzing land use and classification in 2012, but that may not hold for 2013 and 2014.

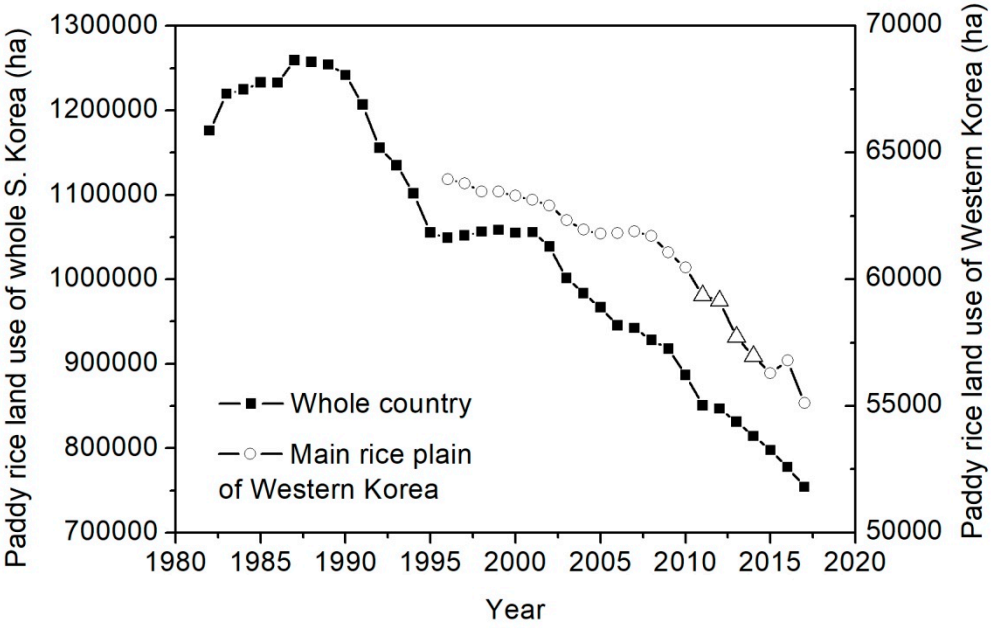

Figure S2. Annual changes of paddy rice land use in main rice plain of Western Korea (open circles from 1995 to 2017, and open triangles from 2011 to 2014) and whole South Korea (filled squares from 1982 to 2017). Data source: KOSIS-STATISTICS KOREA (http://kosis.kr/statHtml/statHtml.do?orgId=101&tblId=DT_1ET0294&language=en&conn_path=I3. * The URL for a statistical table may change in case of the KOSIS revision)

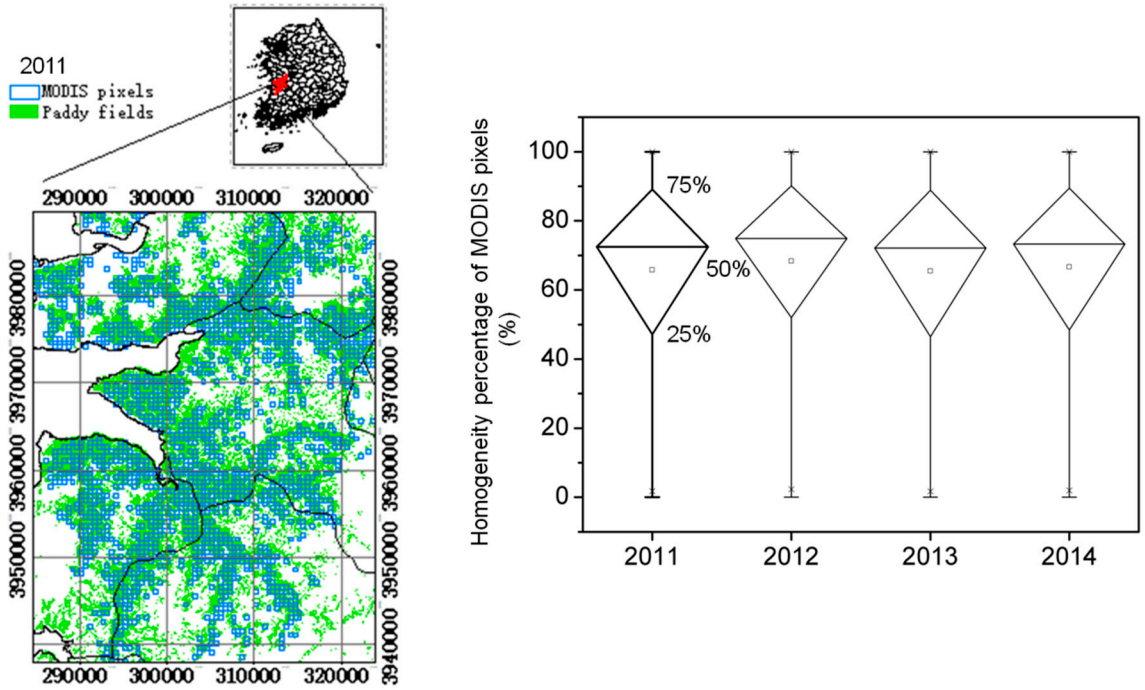

Figure S3. Comparisons between map of MODIS potential paddy pixels (open blue squares) and map of paddy rice land use and cover at 5-m spatial resolution (filled green squares) in the region of Charyeong rice plain (red area in inset), and box charts showing homogeneity percentage of MODIS pixels (i.e.,

percentage of paddy rice area in each MODIS pixel) in 2011-2014 (right-hand column). The 25th, 50th, and 75th percentiles are labeled by 25%, 50%, and 75%, respectively.

SP2. Correlation analysis among $FFTD_{sat}$, gsT_{mean} and *LGP*

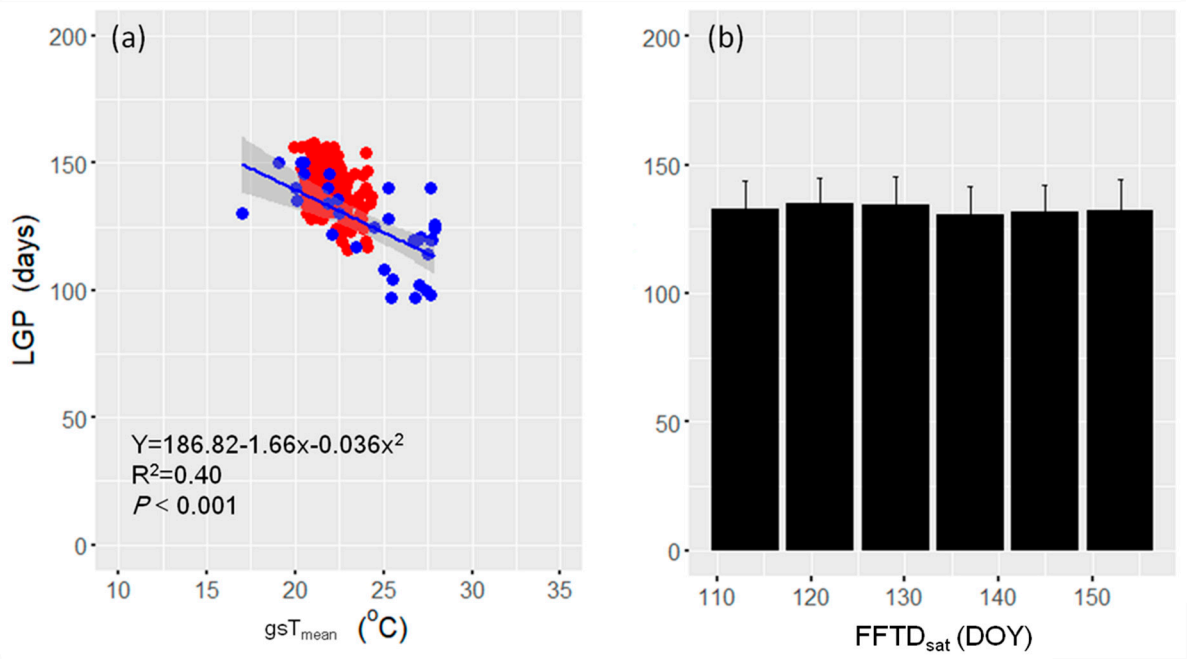

Figure S4. (a) Linear correlation between the length of growing period (*LGP*, days) and mean air temperature of the rice-growing season (gsT_{mean}, °C) and (b) effects of the field first flooding and transplanting date detected by satellite observations ($FFTD_{sat}$) on the *LGP*. *In situ* datasets in blue were acquired from our previous meta-analysis (Xue et al., 2017) and the ones in red were derived from TIMESAT estimations. Shaded band is the 95% prediction interval.

SP3. Algorithm principles of the RS-PM and GRAMI-rice models

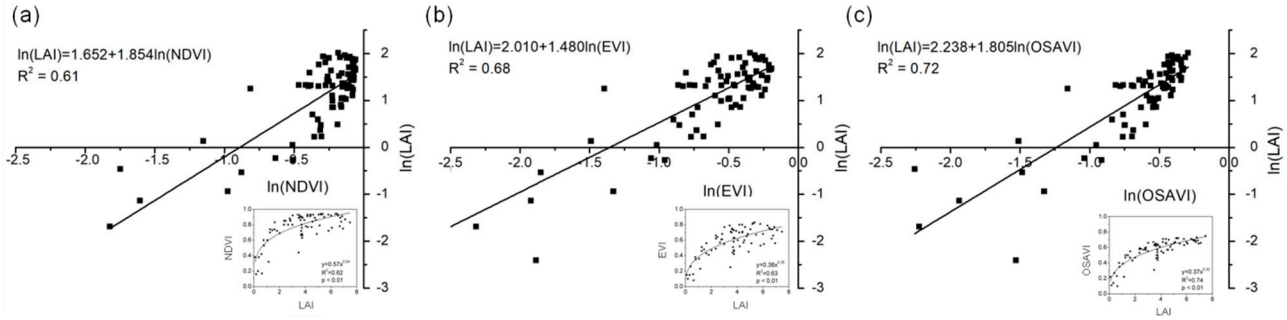

Figure S5. Statistical correlations between (a) ln(*NDVI*) and ln(*LAI*), (b) ln(*EVI*) and ln(*LAI*), (c) ln(*OSAVI*) and ln(*LAI*) in paddy fields in South Korea. Data of *LAI* and *VI*s were processed by natural logarithm. Inset plots show correlations for *LAI-NDVI*, *LAI-EVI*, and *LAI-OSAVI*, respectively.

GRAMI is a crop model based on biophysical processes that uses remotely sensed data and daily weather data and is designed to simulate gramineous crops such as wheat and sorghum and dicotyledons crops like cotton. A derivative of the *GRAMI* for rice has been validated for its capability to reproduce rice field conditions in South Korea (Jeong et al., 2018). The radiation use submodel of the *GRAMI-rice* model is a function of biophysical and meteorological factors (Table S1). Paddy yield was estimated using the harvest index (HI_{AG}, defined as the percentage of the weight of a harvested product by the aboveground plant weight of a crop). Aboveground biomass (*AG*) was added as a subscript of *HI* and radiation use efficiency (RUE_{AG}, dry matter production to the photosynthetically active radiation that is intercepted by plant canopy), as is commonly the case. RUE_{AG} remains conservative in crops grown under non-stress conditions, as justified by Monteith (1977) and Russell et al. (1989). We used a constant RUE_{AG} of 2.3 g DM MJ^{-1} PAR and harvest index of 0.4 for the modern semi-dwarf rice, referring to Mitchell et al. (1998). The *GRAMI-rice* model was applied to estimate biomass production of rice paddies and validated using field observations in the Haean and Gwangju in South Korea, Mase in Japan, and El Saler-Sueca in Spain (Figure S7b).

Table S1. Selected equations involved in the GRAMI-rice model and its description.

Equation	Description
$\Delta D = Max[T - T_b, 0]$	ΔD = daily change in growing degree days, T = daily average air temperature (ºC), and T_b = rice specific base temperature (12ºC)
$\Delta M = \varepsilon \times Q$	ΔM = daily increase in aboveground dry mass (g), ε = rice crop radiation use efficiency (RUE_{AG}), and Q = daily photosynthetic active radiation (PAR, MJ m^{-2}) absorbed by crop canopy
$Q = \beta \times R_s \downarrow \times \left(1 - e^{-k \times LAI}\right)$	Q = absorption of PAR, $R_s\downarrow$ = incident daily solar irradiance (MJ m^{-2}), β = fraction of total solar radiation that is PAR, k = rice crop light extinction coefficient, and LAI = leaf area index

Daily *ET* per rice paddy was estimated with the Penman-Monteith-type *ET* model modified by the Food and Agriculture Organization of the UN (FAO-56 PM model) (Allen et al., 1998). This model estimates *ET* based on a reference crop evapotranspiration (ET_o) multiplied by the sum of transpiration coefficient (K_{cb}) and evaporation coefficient (K_e) of the crop of interest.

$$ET = \left(K_{cb} + K_e\right) \times ET_o \tag{S1}$$

where ET is the actual evapotranspiration (mm m^{-2} day^{-1}), K_{cb} is the crop transpiration coefficient equivalent to the ratio of transpiration to reference evapotranspiration, K_e is the soil evaporation coefficient equivalent to the ratio of soil evaporation to reference evapotranspiration and ET_o is the reference evapotranspiration (mm m^{-2} day^{-1}).

$$ET_o = \frac{0.408 \times \Delta \times \left(R_n - G\right) + \dfrac{\rho_a \times c_p}{\lambda} \dfrac{\left(e_s - e_a\right)}{r_a}}{\Delta + \gamma \times \left(1 + \dfrac{r_s}{r_a}\right)} \tag{S2}$$

Here, R_n is the net radiation (MJ m^{-2} day^{-1}), G is the soil heat flux that is supposed to be neglected when averaged over 24 h or longer time period (Allen et al., 1998; Lee et al., 2011; Alberto et al., 2011; Timm et al., 2014), ρ_a is the mean air density at constant pressure (kg m^{-3}), c_p is the specific heat of the air (MJ kg^{-1} $^oC^{-1}$), λ is the latent heat of water vaporization (MJ kg^{-1}), e_a is the actual vapor pressure (kPa), e_s is the saturated vapor pressure (kPa), r_a is the aerodynamic resistance (s m^{-1}) and r_s is the bulk surface resistance (s m^{-1}). Routines to calculate r_a and r_s were referred to Allen et al. (1998). Crop-specific r_a and r_s were determined by considering the characteristics of rice canopy structure and physiology that regulates r_a and r_s. Growing-season plant height (h, cm) at each paddy pixel was approximated based on estimated LAI (h = 15.0 × LAI), referring to Confalonieri et al. (2011).

The FAO-56 PM model first calculated ET_o for a well-watered and green healthy grass or alfalfa crop by applying recommended physiological parameters for grass and alfalfa. Later, ET for the crop of interest was estimated by multiplying ET_o by the crop coefficient of the crop and its growth stage. This is because crop transpiration and soil evaporation are strongly linked to crop development and the fraction of ground cover. K_{cb} and K_e were estimated based on seasonal daily VI datasets. Daily ET estimation for paddy rice fields of South Korea is made through linking satellite observations and FAO-56 PM model so that ET estimation model here is called remote sensing-based FAO-56 PM model (*RS-PM* model). Seasonal changing profiles of daily K_{cb} representing actual crop growth and development were developed according to time series of $NDVI$, referring to Choudhury (1994) and recommended parameters for paddy rice ecosystems by Nay-Htoon et al. (2018), as follows.

$$K_{cb} = 1 - \left[\frac{NDVI_{\max} - NDVI}{NDVI_{\max} - NDVI_{\min}}\right]^K \tag{S3}$$

where $NDVI_{max}$, $NDVI_{min}$ and $NDVI$ are the vegetation indices for dense canopy, bare soil and green vegetation respectively, and K is the damping coefficient equals 0.59. The K_e of paddy rice was large at the early growth stage when ground cover was minimal, and then rapidly declined with canopy expansion, and finally remained relatively constant at the late growing stage (Nay-Htoon et al., 2018). K_e varies with LAI development. For explicit parameter selection of K_e, a polynomial $NDVI$–K_e correlation (K_e=-0.6024$NDVI^2$ +0.4712$NDVI$+0.7126; Eq. S4) was used when growing degree days (GDD) were < 650ºCd, and when ground cover was small. K_e was assumed to be 0.45 for dense canopy when GDD is > 650ºCd (Eq. S4), referring to Nay-Htoon et al. (2018) and Wei et al. (2018), as follows.

$$K_e = a \times NDVI^2 + b \times NDVI + c \qquad \text{GDD} \le 650^{o}\text{Cd}$$

$$K_e = 0.45 \qquad \text{GDD} > 650^{o}\text{Cd} \qquad \text{(S4)}$$

SP4. EC site information

Haean is located at the northeast of Chuncheon in Gwangwon Province, where rice fields (~501 ha) are grown in the basin. The East Asian monsoon climate prevails during rice growing seasons from June to September, during which the precipitation accounts for over 50% of the annual precipitation. El Saler-Sueca is situated in the protected wetland area “La Albufera Natural Park” in a large rice paddy field area (~1500 ha). It has a Mediterranean semiarid climate with dry and warm summers. Mase in Tsukuba of central Japan has an East Asian monsoon climate similar to the Haean catchment. Detailed site information was tabulated in Table S2. Turbulent and storage CO_2 and H_2O fluxes were logged at a half-hourly interval at the El Saler-Sueca using the standard CarboEurope software (Kutsch et al., 2010), using the EC software package TK2 developed by the Department of Micrometeorology (University of Bayreuth) at the Haean catchment (Zhao and Lüers, 2017) and at the Mase using EC software package JapanFlux in line with the CarboEurope standard (Saito et al., 2005). Grain production at each site was acquired from their publications and via personal communications.

Table S2. Climate conditions at Haean (South Korea), Mase (Japan), and El Saler-Sueca (Spain). T_{ann}: annual mean air temperature; P: annual mean precipitation; EC: eddy covariance system; DOY: day of year.

Study site	Location/Elevation	Climate	Rice planting area	EC data
Haean catchment, S. Korea	38°17′N 128°08′E 450 m	East Asian monsoon T_{ann} = 8.5 ºC P = 1577 mm	ca. 501 ha	From 146 DOY to 274 DOY in 2010, referring to Zhao and Lüers (2017)
Mase, Japan	36°03′14′′N	East Asian monsoon T_{ann} =	ca. 200 ha	From 120 DOY to 276 DOY in

	140°01′38′′E 15 m		13.7 ºC P = 1200 mm		2002, 2003, 2005, referring to Saito et al. (2005)
El Saler-Sueca, Spain	39°16′32′′N 0°18′55′′E 10 m	-	Mediterranean climate T_{ann} = 17.9 ºC P = 550 mm	ca. 1500 ha	From 134 DOY to 270 DOY in 2007, 2008, referring to Kutsch et al. (2010)

SP5. Evaluations of the *RS-PM* and *GRAMI-rice* models

ET underestimation occurred at the early and late growing stages at the Mase site from 2002 to 2005, probably as a result of transient exposure to bare soil surface and removal of aboveground biomass at the harvest stage (Figures S6b-d). Field management practices during the late growing stage (harvest and/or drainage) could substantially affect daily *ET*, which cannot be realized by the current *RS-PM*$_{rs=120}$ model. Daily *ET* at the El Saler-Sueca site from 2007 to 2008 could be well reproduced by the *RS-PM*$_{rs=120}$ model during most of the growing seasons. Large discrepancies between model simulations and eddy flux measurements at this site were found in 2007 and 2008, especially in hot and dry August when daily *VPD* raised over 1.5 kPa (Figures S6e and f), which implies strong impacts of *VPD* on daily *ET* during summer period. Occurrence of *VPD* constraints on daily *ET* was also supported by decline of decoupling factor close to 0.4 during this time period (data not shown here). Average daily air temperature of the rice-growing season for El Saler-Sueca was 22.36ºC, 20.37 ºC in Haean and 21.05 ºC in Mase. Relatively cooler climate existed in Haean and Mase areas as compared to El Saler-Sueca (Table S2). Average values of the rice-growing season *VPD* for El Saler-Sueca, Haean and Mase sites were 2.22, 0.41, and 0.55 kPa, respectively. The average daily *VPD* in El Saler-Sueca area was 4-5 times greater than Haean and Mase sites. Growing season precipitation for the three sites were 279.3, 1165.2, and 684.6 mm. Overall, Mediterranean area had hot and dry summer featured by strong incident radiation and atmosphere driving force for water vaporization from ground surface while East-Asia monsoon area was rainy with less incident radiation and lower *VPD* in summer. We believe that low and moderately high *VPD* is prevailing during the rice-growing season in monsoon South Korea. Overall, there was a close correspondence between field observations and *RS-PM*$_{rs=120}$ simulations across the three sites and measuring years, with a regression close to the 1:1 line. Great fluctuations in daily *ET* observed at the three sites could be well captured by the *RS-PM*$_{rs=120}$ model (Figures S6a-f). Daily *ET* estimations for paddy rice fields by the *RS-PM* model were reasonable. Estimation of paddy production by the adjusted *GRAMI-rice* model was shown against field observations collected at Mase, Haean, El Saler-Sueca, and Gwangju of South Korea (Figure

S7b). A close agreement between simulation and observation for each year/site was arrived with average R^2 = 0.85 and RMSE = 0.23 t ha^{-1}.

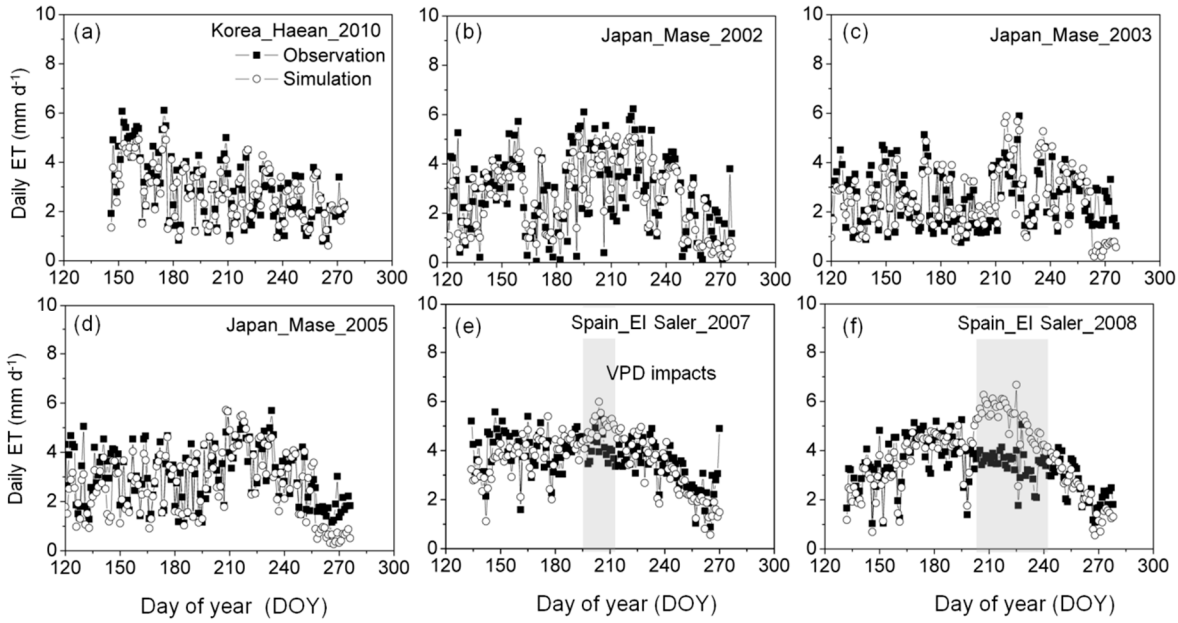

Figure S6. Seasonal changing courses of daily *ET* derived from *EC* systems installed in Haean (a), Mase (b, c, d), El Saler-Sueca (e, f) sites (black squares) and the optimized *RS-PM*$_{rs=120}$ model simulation for each site and year (open circle). Shaded areas in plots e and f indicated potential impacts of intensified *VPD* on daily *ET*. *DOY*: day of year.

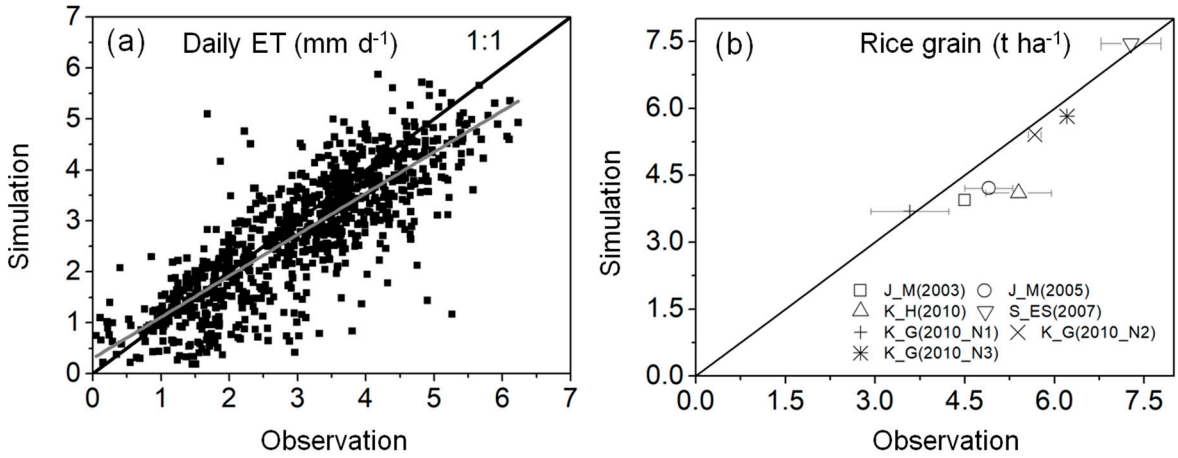

Figure S7. Comparisons between predictions and observations of daily *ET* and grain yield (mean ± SD) in Japan_Mase (J_M), Korea_Haean (K_M), Spain_El Saler-Sueca (S_ES), and Korean_Gwangju (K_G, N1, N2, and N3: 0, 115, and 180 kg N ha^{-1}).

SP6. Temporal variations of evapotranspiration in paddy fields

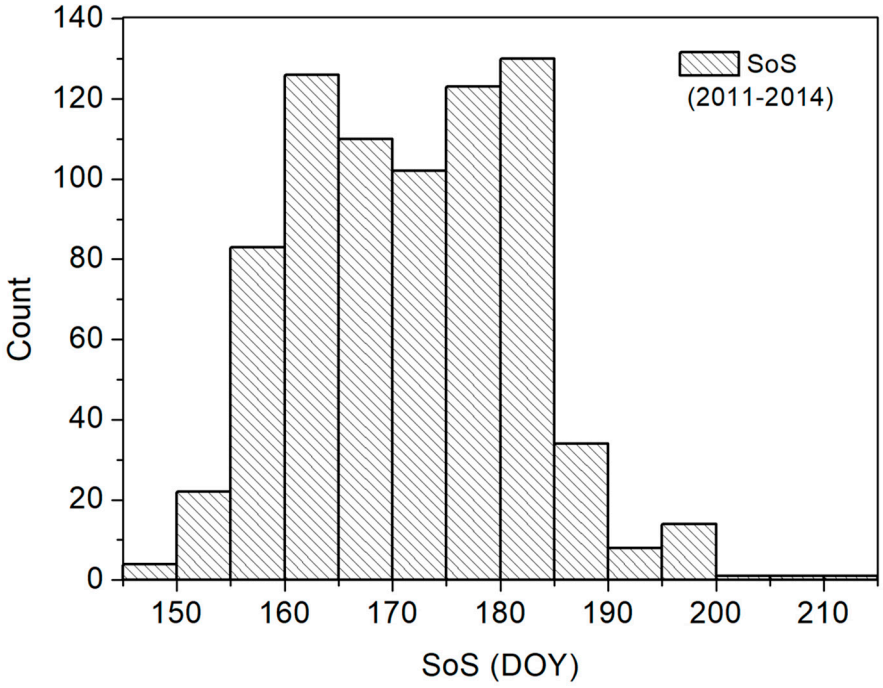

Figure S8. Histogram charts of growing season onset (*SoS*) in paddy fields. Each seasonal metric corresponding to one flood date was the mean over 2011-2014. *DOY*: day of year.

SP7. Response of land surface air temperature to different flooding themes

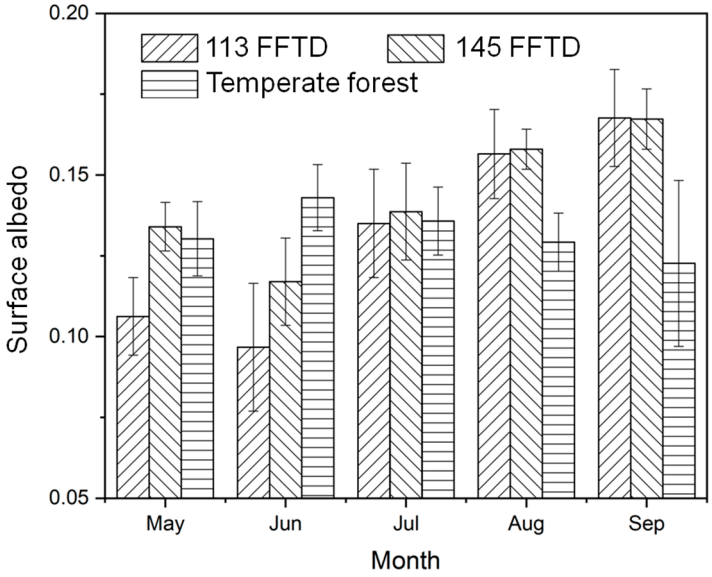

Figure S9. Surface albedo (α) responses to land cover and management change. 113 *FFTD*: first flooding and transplanting date on 113 *DOY*; 145 *FFTD*: first flooding and transplanting date on 145 *DOY*.

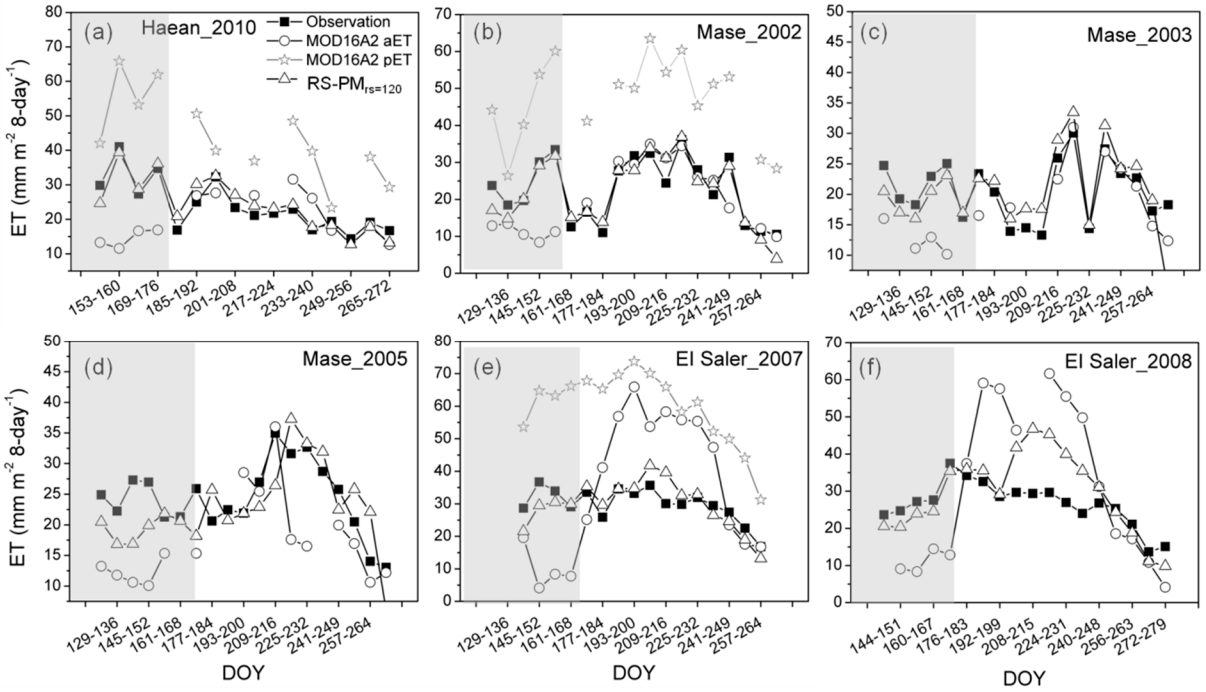

Figure S10. Comparisons of 8-day *ET* of paddy fields in Haean, Mase, and El Saler-Sueca between *EC* observations, MOD16A2 products (*aET* and *pET*: actual *ET* and potential *ET*), and *RS-PM*$_{rs=120}$ simulations. *EC*: eddy covariance system.

SP8. Evaluation of the flooding single-based classification method

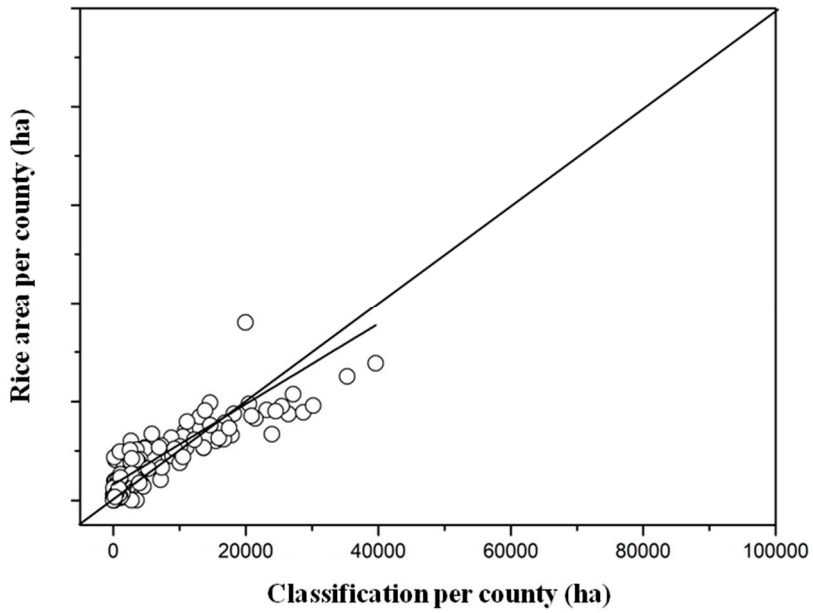

Figure S11. Comparison in paddy rice area per county between national statistic census and estimations by the flooding single-based classification method.

SP9. Spatial distribution of the *FFTD*$_{sat}$ in paddy fields

Table S3. Pearson correlations for the first flooding and transplanting date estimated by satellite observations ($FFTD_{sat}$) and daily air temperature over different time windows. Numerical numbers in the first row were days ahead of the first flooding timing.

	1	2	3	4	5	6	7	8	9	10	11	12	13	14	15
2011	0.76	0.81	0.85	0.86	0.88	0.89	0.92	0.90	0.86	0.86	0.86	0.87	0.85	0.85	0.85
2012	0.69	0.61	0.71	0.77	0.81	0.78	0.79	0.81	0.82	0.82	0.83	0.85	0.85	0.86	0.87
2013	0.94	0.94	0.94	0.94	0.94	0.93	0.90	0.92	0.92	0.93	0.94	0.94	0.94	0.93	0.93
2014	0.37	0.52	0.44	0.27	0.19	0.24	0.30	0.34	0.37	0.36	0.36	0.39	0.44	0.52	0.58

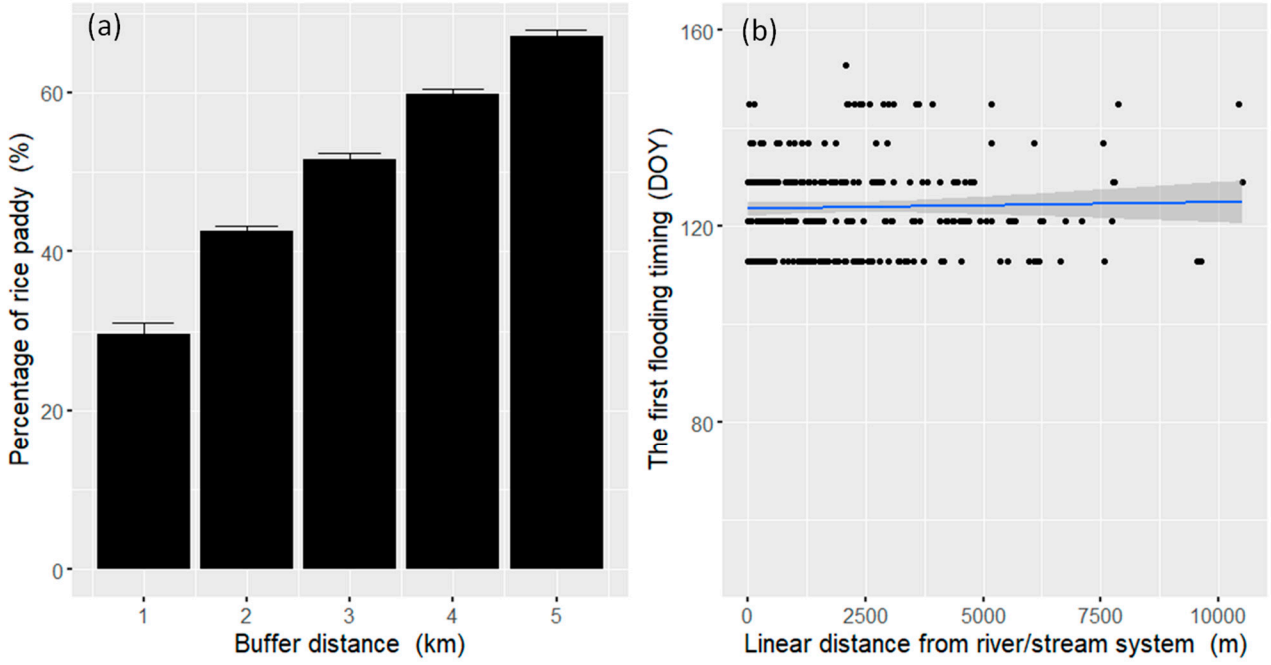

Figure S12. (a) Percentage of rice paddy with buffer distance away from permanent river/stream systems and (b) spatial correlation for the first flooding and transplanting date ($FFTD_{sat}$) and linear distance away from river/stream systems.

SP10. Yield and agronomic water use efficiency (WUE_{agro}) responses to $FFTD_{sat}$

Box charts with yield and *PF-ET* estimations against the $FFTD_{sat}$ are shown in Figure S13. Clumping data of yield/*PF-ET*/WUE_{agro} for each flooding date had a normally distributed population at the 0.05 significance level (Descriptive Statistics-Normality Test). There was no clear ascending or descending tendency in either the 25th, 50th or 75th percentiles of grain yield along with changes in the $FFTD_{sat}$ (Figure

S13a, d, g and j). Rice paddies under different flooding timings had similar grain yields and the differences among their grain yields did not reach statistical significance at the 0.05 level ($p > 0.1$). However, the *PF-ET* was substantially enhanced in paddy fields whose flooding dates had been advanced. In the year of 2012, the *PF-ET* of 153 *DOY*-flooding paddies was ~400 mm, whereas it was ~510 mm at 121 *DOY*-flooding fields (Figure S13e). Substantial increments of the *PF-ET* along with advances in the $FFTD_{sat}$ were also evident in the other three years (Figures S13b, h, k). Although the early flooding paddies produced the same yield as the later flooding ones, the former had a huge water loss of up to 100 mm m^{-2}. This resulted in a lower WUE_{agro} (e.g., 1.1 g grain kg^{-1} water at 121 *DOY*-flooding fields) at the early flooded fields than that of the later flooded fields (1.4 g grain kg^{-1} water at 153 *DOY*-flooding fields).

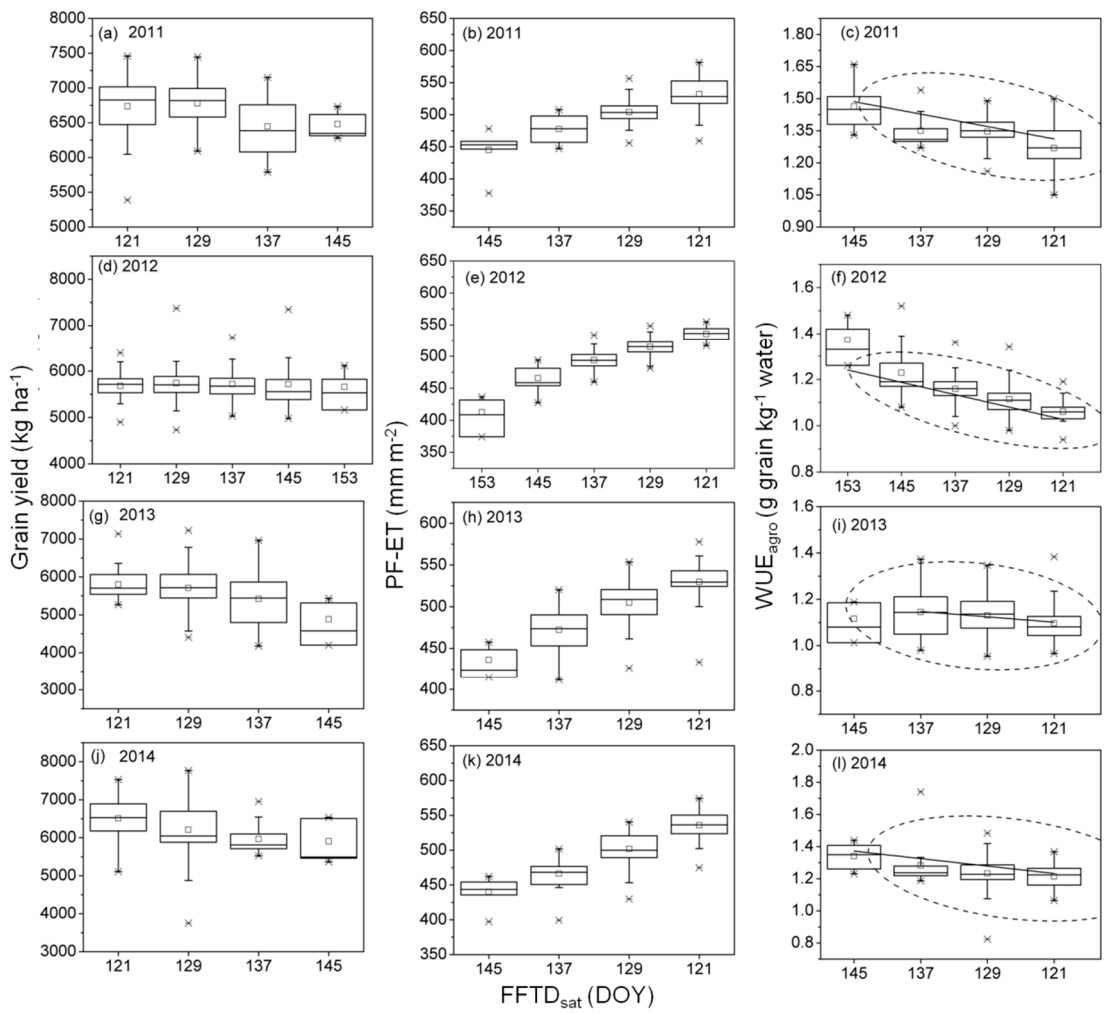

Figure S13. Effects of the first flooding and transplanting date ($FFTD_{sat}$) on grain yield, *PF-ET* and WUE_{agro} in 2011, 2012, 2013 and 2014, South Korea. Dashed ellipses in right-hand column show 95%

confidence level of fitted curves. Box charts in black show the 25th, 50th, and 75th percentiles and maximum/minimum (short hyphen) and mean (open square) values. *DOY*: day of year; *PF-ET*: sum of daily *ET* from the $_{FFTDsat}$ to the end of the rice-growing season; WUE_{agro}: agronomic water use efficiency.

Reference

Allen, R.G., Pereira, L.S., Raes, D., Smith, M., W, A.B. 1998. Crop evapotranspiration-Guidelines for computing crop water requirements-FAO Irrigation and drainage paper 56. Irrig. Drain., 1–15,.

Confalonieri, R., Bregaglio, S., Rosenmund, A.S., Acutis, M., Savin, I., 2011. A model for simulating the height of rice plants. Eur. J. Agron. 34, 20-25.

Choudhury, B.J., 1994. Synergism of multispectral satellite observations for estimating regional land surface evaporation. Remote Sens. Environ. 49, 264–274.

Jeong, S., Ko, J., Yeom, J.M., 2018. Nationalwide projection of rice yield using a crop model integrated with geostationary satellite imagery: A case study in South Korea. Remote Sens. 10, 1665, doi:10.3390/rs10101665.

Kutsch, W.L., Aubinet, M., Buchmann, N., Smith, P.J., Osborne, B., Eugster, W., Wattenbach, M., Schrumpf, M., Schulze, E.D., Tomelleri, E., 2010. The net biome production of full crop rotations in Europe. Agric. Ecosyst. Environ. 139, 336-345.

Mitchell, P.L., Sheehy, J.E., Woodward, F.I., 1998. Potential yield and the efficiency of radiation use in rice. IRRI Discussion Paper Series No.32. Manila (Philippines): International Rice Research Institute. p 62.

Monteith, J.L., 1977. Climate and the efficiency of crop production in Britain. Philos. T. R. So. B. 281, 277–294,.

Nay-Htoon, B., Xue, W., Lindner, S., Cuntz, M., Ko, J., Tenhunen, J., Werner, C., Dubbert, M., 2018. Quantifying differences in water and carbon cycling between paddy and rainfed rice (Oryza sativa L.) by flux partitioning. PLOS ONE 13, e0195238.

Russell, G, Jarvis, P.G., Monteith, J.L., 1989. Absorption of radiation by canopies and stand growth. In: Russell G, Marshall B, Jarvis PG, editors. Plant canopies: their growth, form and function. Society for Experimental Botany Seminar Series 31. Cambridge, Cambridge University Press, p 21–39.

Saito, M., Miyata, A., Nagai, H., Yamada, T., 2005. Seasonal variation of carbon dioxide exchange in rice paddy field in Japan. Agr. Forest Meteorol. 135, 93-109.

Wei, Z., Lee, X., Wen, X., Xiao, W., 2018. Evapotranspiration partitioning for three agro-ecosystems with contrasting moisture conditions: a comparison of an isotope method and a two-source model calculation. Agri. Forest Meteorol. 252, 296-310.

Xue, W., Lindner, S., Dubbert, M., Otieno, D., Ko, J., Muraoka, H., Werner, C., Tenhunen, J., 2017. Supplement understanding of the relative importance of biophysical factors in determination of photosynthetic capacity and photosynthetic productivity in rice ecosystems. Agri. Forest Meteorol. 232, 550-565.

Zhao, P., Lüers, J., 2017. Parameterization of evapotranspiration estimation for two typical East Asian crops. Atmosphere 8, 111.